## ABSTRACT

PATEL, MAHARSHI NIMESH. Autonomous Robotics for Invasive Aquatic Plant Management. (Under the direction of Dr. Gregory D. Buckner).

Invasive aquatic plant species can expand rapidly throughout water bodies and cause severely adverse economic and ecological impacts. While mechanical, chemical, and biological methods exist for the identification and treatment of these invasive species, they are manually intensive, inefficient, costly, and can cause collateral ecological damage. To address current deficiencies in aquatic weed management, research focused on the development of a small fleet of fully autonomous boats capable of subsurface hydroacoustic imaging (to scan aquatic vegetation), machine learning (for automated weed identification), and herbicide deployment (for vegetation control). These capabilities aim to minimize manual labor and provide more efficient, safe (reduced chemical exposure to personnel), and timely weed management. Geotagged hydroacoustic imagery of three aquatic plant varieties (Hydrilla, Cabomba and Coontail) is collected and used to create a software pipeline for subsurface aquatic weed classification and distribution mapping. Employing deep learning, the novel software achieves a classification accuracy of 99.06% after training.

# Autonomous Robotics for Invasive Aquatic Plant Management

by
Maharshi Nimesh Patel

A thesis submitted to the Graduate Faculty of
North Carolina State University
in partial fulfillment of the
requirements for the degree of
Master of Science

Mechanical Engineering

Raleigh, North Carolina
2019

APPROVED BY:

| | |
|---|---|
| _____ | _____ |
| Dr. Andre Mazzoleni | Dr. Scott Ferguson |

_____
Dr. Gregory Buckner
Chair of Advisory Committee

## BIOGRAPHY

Maharshi Nimesh Patel was born and raised in India. He completed his Bachelor of Technology in Mechanical Engineering from Nirma University, Ahmedabad, India in 2015. After working for two years in the automotive industry, he decided to further his studies and began work on his master's degree in the department of Mechanical and Aerospace Engineering. Currently, he works at the Electro-Mechanics Research Laboratory under the direction of Dr. Gregory Buckner, pursuing research interests in autonomous robotics.

## ACKNOWLEDGMENTS

I would like to thank my parents for always supporting me and giving me the encouragement to keep trying during rough times. Special thanks to Megha for always standing by me. A word of thanks to all friends and family members without whom none of this would have been possible.

I would like to thank my advisor, Dr. Gregory Buckner, for giving me an opportunity to work as a Research Assistant under his guidance and support. I would also like to thank Shaphan Jernigan, Eric Stewart, Gordon Beverly, Esther Lee, Dr. Rob Richardson, Steve Hoyle, Andrew Howell and Tyler Harris for the success of this project. I am grateful to Dr. Scott Ferguson for being my advisory committee member along with his help in the research.

My sincere thanks to Dr. Andre Mazzoleni for providing continuous guidance throughout my Master's, besides being my advisory committee member. My thanks to the members of the Crop Science department, the Electro-Mechanics Research Laboratory and the Engineering Mechanics and Space Systems Laboratory.

This research was completed with the technical and financial support from United Phosphorus Inc. and a generous funding from the North Carolina Policy Collaboratory.

## TABLE OF CONTENTS

## LIST OF FIGURES

# CHAPTER ONE:

# INTRODUCTION

## 1.1 Impact and Treatment of Aquatic Weeds

While native aquatic plants are essential components of aquatic ecosystems, non-native invasive species can expand rapidly throughout water bodies and cause severe economic and ecological impacts (Fig. 1). Adverse economic impacts include impairing recreational activities (fishing, swimming and boating); flooding caused by reduced drainage; hindering boat navigation; blocking water intakes for hydroelectric turbines, drinking water, and irrigation; and reducing the potability of fresh water due to foul taste and odor. Indirect economic effects include reduced property values and reduced revenue from impacted businesses. Aquatic flora consume oxygen at night; thus, excessive weed growth can deprive fish and other aquatic animals of this vital resource, leading to their death. Other ecological effects include overpopulation of small fish, which find shelter in the plants, and the creation of breeding habitats for some mosquito species. Of the many invasive aquatic plant species, *hydrilla verticillata*, commonly known by its genus hydrilla, likely causes the most economic damage in the United States.

Given these adverse impacts, management of invasive aquatic vegetation is of utmost concern. While mechanical control (plucking or raking the plants) is the most direct approach, it can be time-consuming and costly (estimated cost of $1,000 per acre in 1996 [Langeland 1996]). Biological control methods (e.g. fish which consume large quantities of aquatic weeds) are routinely employed but can be counter-productive. One example, the grass carp, can consume and

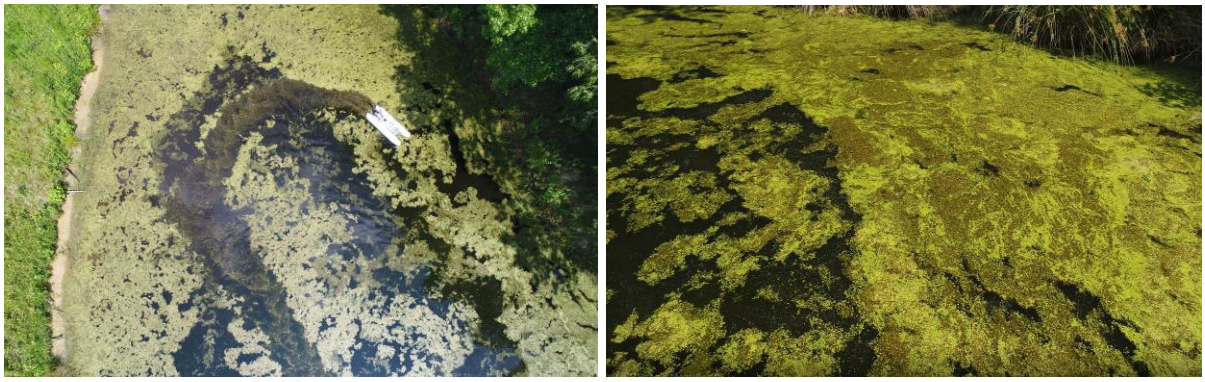

*a)* *b)*

*Figure 1*. Watermeal infestation in a central North Carolina pond: a) aerial view; b) ground view.

control vegetation; however their body waste compromises water quality, killing sensitive plant and animal species and fertilizing additional weed growth. Biological approaches also introduce the risk of invasive animal species [Helfrich 2009]. Seven species of carp native to Asia, introduced to control invasive plant species, have recently spread up the Mississippi River system and have crowded out native fish populations. While not without its drawbacks, chemical control (the application of herbicides) is considered the most attractive aquatic weed management method in terms of minimizing cost, time and collateral damage [C. Lembi, 2009].

Efficient chemical-based vegetation control in aquatic bodies requires proper identification and quantification of the extent to which vegetation is present, both for optimal chemical selection and treatment strategies. The approach of manually identifying weed-infested regions within a water body and applying herbicides at the target location(s) is labor intensive, time consuming and involves risk of herbicide exposure to personnel. Spraying herbicide throughout the water body leads to much higher usage, resulting in economic loss, longer decomposition times, and subsequent environmental hazards.

## 1.2 Application of Machine Learning for Vegetation Monitoring

Automated plant identification, which relies on photographic images, is a well-developed methodology for agricultural applications. With recent advances in artificial intelligence, several machine learning algorithms have been developed for image classification. Current identification/classification methods involve image preprocessing followed by feature extraction. The extracted features, which typically include the color, shape and texture of leaves, Histograms of Oriented Gradients (HOG), etc., are then used to train classifiers. This approach has been applied to plant identification by acquiring photographic images of leaves, performing the image preprocessing operations shown in Figure 2, and extracting features from the modified images [S. J. Kho, et. al, 2017]. These authors implemented Support Vector Machines (SVMs) and Artificial Neural Networks (ANNs) separately as classifiers. A similar approach was adopted by another group of researchers to identify aquatic weeds growing on the water surface [L. Pereira, 2012]. Visible light images captured from Unmanned Aerial Vehicles (UAVs) were utilized to train multiple classifiers. In addition to SVM, Optimum-Path Forest classifiers (OPF) and Bayesian classifiers were investigated.

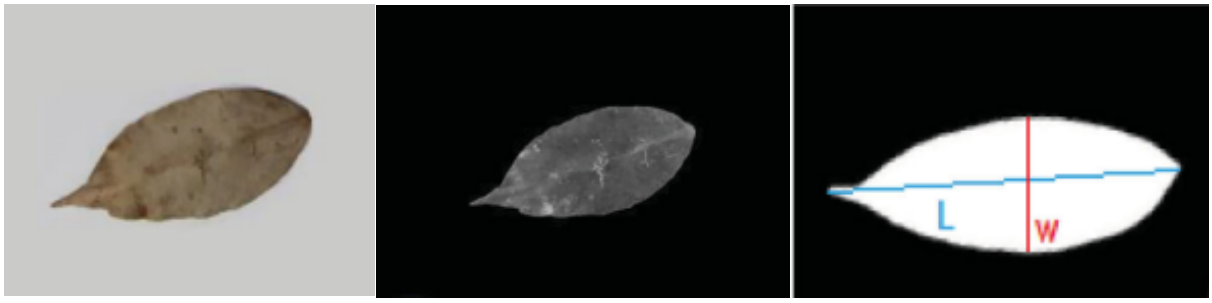


*a)* *b)* *c)*

*Figure 2.* Feature extraction from an image of a leaf [S. J. Kho, 2017] a) Clear image of a leaf; b) Grayscale image of the leaf; and c) Feature extraction after identifying boundaries of the leaf.

In similar research, feature learning on high resolution weed images was performed using a filter bank, followed by image classification via the texton approach (K-means clustering). [Hung, Xu, & Sukkarieh, 2014]. Feature extraction and OPF classifiers were successfully implemented in another study to identify invasive yellow flag iris plants. [Baron, Hill, & Elmiligi, 2018].

Despite the documented success of these feature extraction-based plant classification methods, they cannot be directly applied to subsurface plant identification due to limited visibility and associated lack of photographic clarity. Despite lacking the resolution and clarity of photography, hydroacoustic imaging is an emerging option for the quantification of underwater vegetation. Currently, hydroacoustic data files can be uploaded and processed offline via a web-based service (Navico BioBase), which generates biomass-concentration maps. However, the limited resolution of hydroacoustic data impedes feature extraction and typical machine learning approaches to species classification.

Deep learning is a more advanced machine learning technique that could overcome these limitations. It employs Deep Neural Networks (DNNs) to simultaneously accomplish feature extraction and classification tasks. The fundamental component of a DNN is an Artificial Neural Network (ANN). As shown in Figure 3, a standard feedforward ANN consists of multiple fully connected layers (input, hidden, and output layers); each layer consists of varying number of nodes (artificial neurons) depending on the complexity of the network. The input layer $X = [x_1, x_2, \ldots x_n]^T$ takes n extracted features (or pixel values of images), which are multiplied by an adaptable weight matrix $W^1 = [w_{11}^1, w_{12}^1, ..., w_{1h}^1; ...; w_{n1}^1, ..., w_{nh}^1]$, where h is the number of neurons in the hidden layer. These values are multiplied by another adaptable weight matrix $W^2 = [w_{11}^2, w_{12}^2, ..., w_{1m}^2; ...; w_{h1}^2, ..., w_{hm}^2]$, where m is the number of ANN outputs $Y = [y_1, y_2, \ldots y_m]^T$.

Each ANN output corresponds to a specific classification (m classes in this case). By incorporating non-linear activation functions in the output layer neurons (e.g. softmax or sigmoid), the output layer values can be transformed to predict the species classification for an input image. ANN weights are randomly initialized and optimized through a repetitive training process.

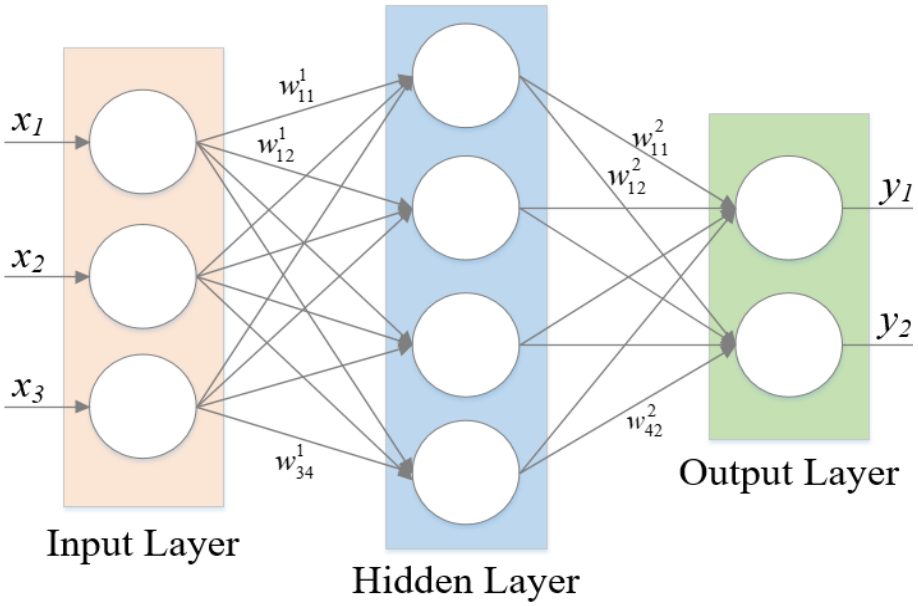


*Figure 3.* Architecture of an Artificial Neural Network.

ANN or DNN training involves two processes: Forward propagation and Backward propagation. Inputs of known classes are used during these processes. Forward propagation produces the predicted output. The probability of each class is calculated using sigmoid function *(σ(x))* on the output layer matrix $\hat{Y}$ (in equations, $Y$ is considered to be the matrix with actual output values and $\hat{Y}$ as the predicted output). This is obtained from hidden layer matrix $H$ and input layer matrix $X$. The computation is explained in equations 1.1-1.3; where $B^1$ and $B^2$ are bias matrices. The sigmoid function can be replaced by softmax function according to the application (Sum of all outputs of softmax function is one, making it preferable for multi-class classification).

$$\hat{Y} = \sigma(H^T W^2 + B^2) \tag{1.1}$$

$$H^T = X^T W^1 + B^1 \tag{1.2}$$

$$\sigma(x) = \frac{1}{1+e^{-x}} \tag{1.3}$$

Backward propagation includes iterative optimization of the weights to produce accurate results during output prediction. The computations (1.4-1.8) include updating all the weights across all layers using gradient based approaches. Gradients are calculated from the error function (*E(W)*) which is a comparison between predicted output ($\hat{Y}$) and actual output values (*Y*). $\alpha$ is the learning rate for updating weights (1.4).

$$w_{ij}^{'k} = w_{ij}^{k} - \alpha \frac{\partial E}{\partial w_{ij}^{k}} \tag{1.4}$$

$$\frac{\partial E}{\partial w_{11}^{2}} = \frac{\partial E}{\partial \hat{y}_1} . \frac{\partial \hat{y}_1}{\partial w_{11}^{2}} \tag{1.5}$$

$$\frac{\partial E}{\partial w_{11}^{1}} = \frac{\partial E}{\partial \hat{y}_1} . \frac{\partial \hat{y}_1}{\partial h_1} . \frac{\partial h_1}{\partial w_{11}^{1}} \tag{1.6}$$

$$\sigma^{'}(x) = \frac{1}{1+e^{-x}} . \frac{e^{-x}}{1+e^{-x}} = \sigma(x)(1-\sigma(x)) \tag{1.7}$$

$$E(W) = -\frac{1}{m} \sum_{i=1}^{m} \{ y_i . \ln(\hat{y}_i) + (1-y_i) . \ln(1-\hat{y}_i) \} \tag{1.8}$$

Unlike standard ANNs, DNNs integrate feature extraction by incorporating several additional layers [Y. Sun et al., 2017]. Convolutional Neural Networks (CNNs, Fig. 4), one of the most popular subtypes of DNNs, replace matrix multiplication with convolution in the initial layers. Instead of multiplying all inputs (pixels of image) with different weight sets, a small window of inputs is multiplied by a weight set and the window is iteratively shifted to cover entire input matrix (image) while using the same weights. This decreases the number of weights and

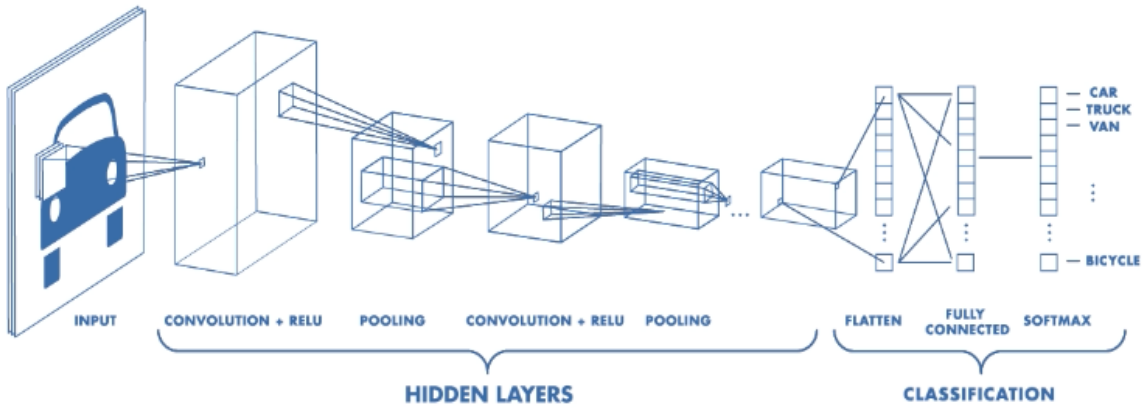


*Figure 4.* Architecture of a Convolutional Neural Network (CNN) [www.mathworks.com].

reduces network complexity and associated preprocessing[Liu et al., 2017]. However, with significantly deeper structures (as compared to ANNs), CNNs and other DNNs have significantly larger numbers of learnable parameters. Consequently, DNN training is computationally intensive and has only recently become viable due to advances in computer processing. After training, however, DNNs can be utilized for real-time image classification with minimal processor capabilities.

## 1.3 Research Objective

To address current deficiencies in aquatic weed management, this research seeks to develop and demonstrate a small fleet of fully autonomous boats capable of subsurface hydroacoustic imaging (to scan aquatic vegetation), machine learning (for automated weed identification), and herbicide deployment (for vegetation control). These capabilities aim to minimize manual labor and provide more efficient, safe (reduced chemical exposure to personnel), and timely weed management. The development of autonomous boats was contracted by United Phosphorous, Inc., and completed by a team of researchers at N.C. State. These boats provided a platform for

hydroacoustic data acquisition and the development of machine learning algorithms, the primary focus of this thesis, which was funded by a N.C. Policy Collaboratory grant.

# CHAPTER TWO:

# METHODS

## 2.1 Autonomous Boat Development

The first phase of R&D was the design and fabrication of water vehicles which provided the following functionality: fully autonomous navigation, coordination between at least two vehicles, hydroacoustic data collection, variable rate herbicide application, and at least two hours of continuous operation without refuel/recharge (Fig. 5). For practical purposes, a surface vehicle, rather than a submarine platform, was chosen. Other design choices included the use of a 15-gallon (56.8 liter) herbicide tank, a seemingly ideal volume for the targeted market segment; electric propulsion; and battery-based energy storage. Additional design considerations and details are presented below.

*Figure 5.* Autonomous boat prototype for identification and chemical treatment of invasive aquatic plant species.

### *2.1.1 Hull Design and Fabrication*

A multi-hull vee-shaped design was selected for each vehicle, among other options (deep vee, round bottom, flat bottom, etc.). Multiple hulls provides maximum stability, while the vee shape produces relatively low drag in displacement mode. Scanning operations are optimal at lower speeds (0.5-1.5 m/s), obviating any need for planning-optimized hull designs (deep vee and flat bottom). With the use of hydrostatic analysis, pontoon dimensions were computed to support the geometry and weight of fully loaded payload components (batteries, electronics, herbicide tank filled to 15 gallon capacity, electronics, propulsion system, etc.) with 50% or less pontoon submersion [Beverly 2017]. The resulting geometry of each pontoon was 244 × 26 × 30 cm (96.0 × 10.2 × 11.9 in), not including keel dimensions.

To speed the development and evaluation processes, initial hull prototypes were fabricated from polystyrene foam. The process involved adhering sheets of the material to each other and sanding and trimming them to the desired geometry. These provided adequate floatation but lacked robustness to impacts with other structures during boat handling and water body navigation.

After basic functionality was demonstrated, the polystyrene pontoons were replaced with custom-made fiberglass pontoons of similar geometry. Production of fiberglass pontoons was a multi-step process. Firstly, a polystyrene foam plug, representing the left half of the pontoon geometry was fabricated (Fig. 6 a-b). A fiberglass epoxy-resin-based mold (negative) was then formed over the plug (Fig. 6c). Similarly, a plug and mold were fabricated for the right half of the pontoon (mirrored geometry) and the two fiberglass mold halves bolted to each other (Fig. 6d) to form a complete mold. Finally, each pontoon was formed within the mold (Fig. 6e). Pontoon caps were fabricated using a separate mold (Fig. 6f). A keel was integrated into the base of the pontoons for improved boat tracking. Multiple coats of polyester resin and liquid rubber were applied to the


*Figure 6.* Fabrication of fiberglass pontoons: a) cutting, sanding, and bonding polystyrene plug sections; b) epoxy coating, sanding, and gel-coating of plug; c) fiberglass lay-up of mold over polystyrene plug; d) assembly of mold halves (shown with keel upward); e) fiberglass pontoon after lay-up inside mold an application of multiple finish coats; and f) separately cast pontoon cap installed.

surface of the pontoons and caps for enhanced waterproofing and cosmetics. The frame of the boat was fabricated from aluminum struts, which were waterjet-cut from sheets, bent to final geometry, and bolted between and within the pontoons (Fig. 7). The struts provided enhanced lateral support and load-bearing capabilities. The fore and aft regions of the fiberglass pontoons were filled with

low-density (32 kg/m$^3$ or 2 lbf/ft$^3$) urethane foam to provide buoyancy and prevent sinking of the boat, even in cases of capsizing or other scenarios involving flooding of the pontoons. The middle regions of the pontoons were partially filled with this foam to cradle the batteries (one per each side) and a bin containing electrical components. Hatch doors with water-resistant draw latches were installed above this region to allow easy access to the batteries and electronics for battery recharging and electronics troubleshooting.

*a)* *b)*

*Figure 7.* a) Aluminum struts bolted within the pontoons for enhanced lateral support (before foam filling); b) urethane foam filling process.

### *2.1.2 Propulsion and Steering*

Airboat-type propulsion, consisting of an aircraft propeller driven by a brushless DC motor, was implemented in early prototypes, owing to its reduced risk of entanglement with sub-surface aquatic plants and consequent ability to operate at minimal water depths. Steering was achieved through placement of the propeller/motor assembly on an RC-servo-actuated rotating

platform, which could swivel ± 45° from the neutral position (Fig. 8a). This design was capable of a boat turning radius of 0.2 m, as measured from GPS telemetry data.

In spite of its steering ability, the aircraft-propeller-based system was thrust-limited and inefficient with regards to power consumption. Its final configuration, implementing a 0.41 m aircraft propeller and 1200-W brushless DC motor (Fig. 8a), yielded a maximum thrust of only 22.7 N. In lake tests, the under-powered boat could reach a maximum speed of only 1.2 m/s, and its navigational ability was subsequently highly sensitive to wind and wave disturbances. Usage was limited to relatively calm days (winds of 2.2 m/s, 5 mph, or less,). Furthermore, the high rotational speed of the propellers (6,000+ rpm) produced a high level of noise. Substantial gains in thrust and elimination of noise disturbances were achieved by replacing the airboat-based propulsion system with an off-the-shelf marine propulsion unit (Fig. 8b, Minn Kota Powerdrive 45, Johnson Outdoors, Racine, WI, 200.2 N thrust rating). It was determined the shallow water benefits of the airboat system were outweighed by the substantial increases in thrust and efficiency of the marine propeller. For remote steering, the factory-installed steering motor was interfaced with a motor controller with RC input and feedback capabilities (Pololu Jrk 12v12, Pololu Corporation, Las Vegas, NV). Measurement of the shaft position for closed-loop control was implemented through a custom-mounted potentiometer rotationally coupled to the shaft via mechanical gears on each of these components (Fig. 8c). A translating, spring-loaded frame and oversized gear teeth accommodated bow-to-stern shaft wobble, inherent in the system, to maintain gear meshing and avoid damage to the potentiometer.

### *2.1.3 Navigation and Control Unit*

At a minimum, autonomous navigation requires a GPS receiver and magnetic compass for localization (sensing position and heading) and processor for maintaining real-time closed-loop

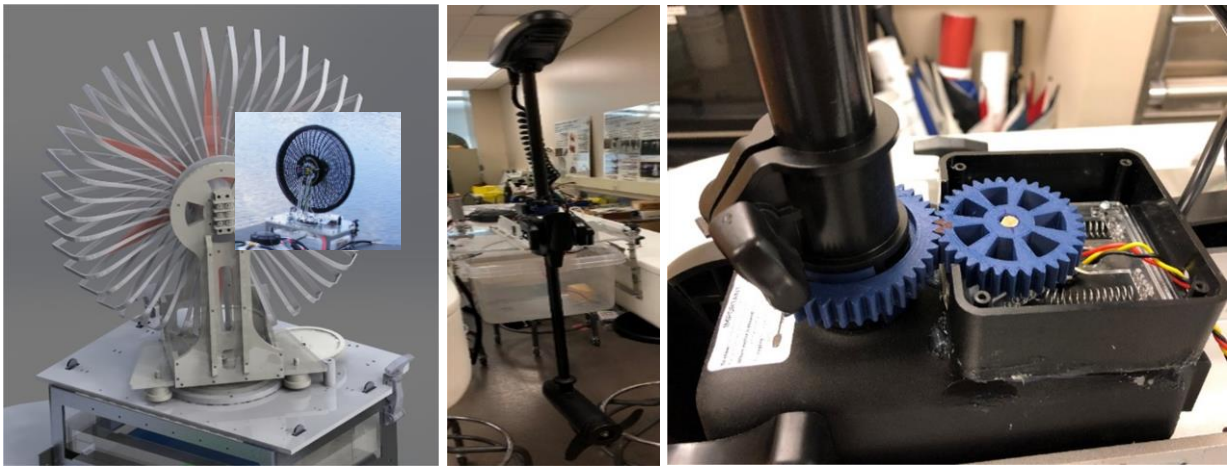

*a)* *b)* *c)*

*Figure 8.* Steering and propulsion systems: a) CAD model and photograph (inset) of aircraft-propeller-based system of preliminary prototypes, b) Minn Kota marine propulsion unit, and c) rotational potentiometer used for shaft position feedback.

control of steering and propulsion systems. A wireless transmitter/receiver with reasonable transmission range is also needed for communication with a base station and other autonomous vehicles in the fleet. The Pixhawk autopilot module, an open-hardware device originally manufactured by 3DR (3DR, Berkeley, CA), was selected from the available alternatives for its widespread usage and support community and its compatibility with a wide range of sensors and software (Fig. 9a). Mission Planner open-source software, installed on a standard notebook computer (Dell Latitude 5550, Windows 7 OS), coupled with USB-based telemetry radios, served as the primary on-shore interface between the human operator and the onboard autopilot module (Fig. 9b). User-configurable remote control transmitters (FrSky Taranis X9D Plus, FrSky Electronic Co., Limited, Jiangsu, China), each paired with an X8R receiver aboard each vehicle, could be used for direct control of a vehicle as desired (launching, object avoidance, etc.). Toggling a transmitter switch instantly alternated between autonomous and manual control modes for the corresponding vehicle.

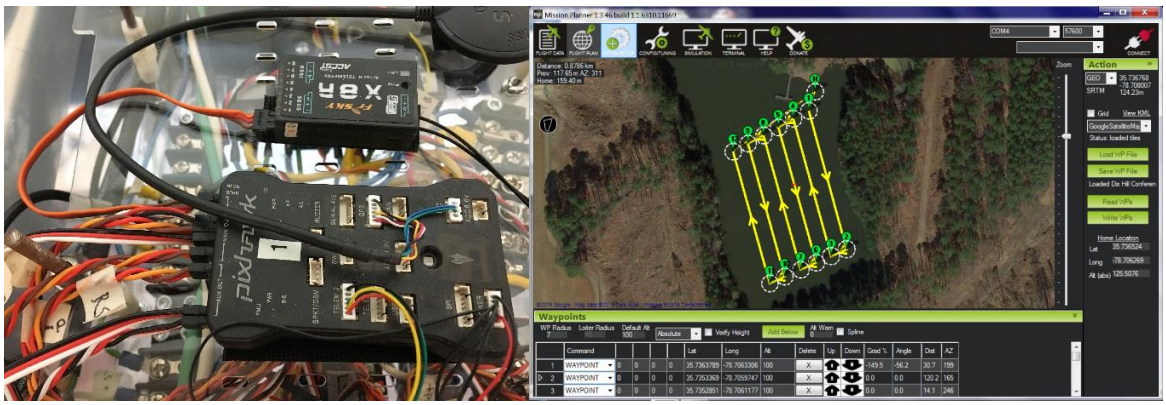

*a)* *b)*

*Figure 9.* Features utilized for autonomous vehicle control: a) Pixhawk autopilot module as installed within a prototype (receivers and other electronics in background) and b) Mission Planner interface showing generation of transects.

Hydroacoustic mapping for weed quantification typically involves navigation of a watercraft through a series of parallel linear trajectories, commonly known as transects, spread throughout the target region (Fig. 9b). Such navigation requires tracking accuracy. Transects, compiled within Mission Planner, were loaded to the module via telemetry communication. From the Mission Planner interface, the operator can also remotely adjust autonomous navigational control parameters, as well as monitor navigational performance in real-time (actual vs. desired trajectories, velocity, heading, etc., Fig. 10). The autopilot module implements a version of L1 trajectory tracking [S. Park, 2004]. In this method, a reference point "L1_ref" on the desired trajectory is calculated, and the vehicle is directed (through steering inputs) towards that point (Fig. 10). L1 tracking period, a key user-defined parameter, determines the aggressiveness of the vehicle in reaching the L1_ref point. The reference point is kept sliding constantly along the required trajectory. Due to trade-offs in parameter tuning, e.g., increasing gains can lead to oversteering and weaving, the parameters (primarily L1 tracking period and PID components) were fine-tuned with intensive experimentation.

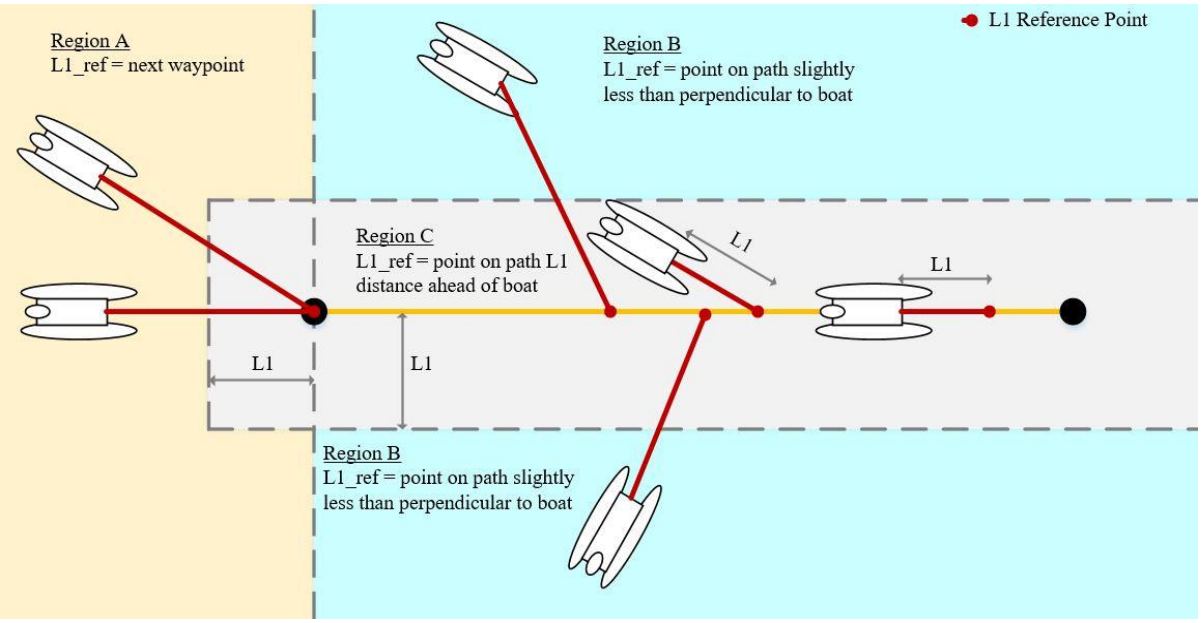


*Figure 10.* L1 tracking schematic showing computation of reference point (L1_ref) at various vehicle positions with respect to the desired path [B. Jones, 2013].

### *2.1.4 Herbicide dispersal system*

For design of the herbicide dispersal system, hydrilla was chosen as the targeted aquatic weed; Aquathol-K, a liquid-based chemical effective in the treatment of hydrilla and other aquatic weeds, was selected as the treatment herbicide. A downstream chemical dilution system, with a drop hose outlet and an RC-controlled (via ESC) variable-speed pump, was utilized for dispersal. With this design, herbicide concentrate is stored within an onboard tank, diluted with water drawn from the lake, and dispersed through a hose submerged below the water surface. Dilution occurs at an injector downstream the pump, which passively combines concentrate with lake water via the Venturi effect. Fluid analysis of the dispersal system and a series of tests were conducted for pump selection (8000 series SHURflow industrial pump, 100 psi rating) and to characterize chemical dispersal rates as a function of RC input (Fig. 16). These relationships allowed optimal RC pump control inputs to be determined as a function of transect spacing, boat velocity, desired

application rate, and lake depth. Dispersal system design and analysis is further detailed in [Beverly 2017].

Design optimization methodologies, incorporating Stevin's law of fluid statics, were used to optimize the placement of onboard components (batteries, electronics bin, chemical tank, propulsion system, dispersal pump, etc.). The objective of the algorithm, implemented with Excel Solver, was to minimize pitch angle of the boat throughout all levels of tank payload (empty to full); a key constraint was avoidance of forward pitching (bow pitched downward). The methods and results, as detailed in [Beverly 2017], were adapted for later prototype generations as component dimensions, weights, and placement options, e.g., component storage within the pontoons, were altered.

#### *2.1.5 Hydroacoustic Imaging*

An off-the-shelf hydroacoustic imaging system (Lowrance Elite 4 Chirp, Lowrance Electronics, Tulsa, OK) was purchased and integrated within each boat. Its transducer was silicone-mounted within the base of a plastic container at the fore region of the boat. The unit allowed geo-tagged transducer data to be stored on a microSD card in .sl2 file format.

## 2.2 Machine Learning for Aquatic Vegetation Classification

The second phase of the project involved the development of automated methods for classifying and quantifying aquatic weeds, and successively utilizing this data to determine locations for targeted herbicide treatment.

### *2.2.1 Data Preprocessing*

The acquired .sl2 data, being in a binary format with no manufacturer manufacturer-provided tools or guidelines for opening and reading the contents, could not be directly used for classification using machine learning classification algorithms. To convert this .sl2e data into a series of standard digital images (.jpg format) with geotagging, a two-step approach was used. First, the .sl2 file was opened/read using Reefmaster Sonar Viewer (ReefMaster Software Ltd., West Sussex, U.K.), a software program that enables the display of directly suited for displaying sonar data (hydroacoustic imagery and corresponding geographical location) in a continuous video form, similar to a video. Figure 11 is a screenshot of hydroacoustic data recorded at Lake Raleigh viewed using the "Reefmaster Sonar Viewer" software. "Primary" and "DownScan™" images are displayed along with a map indicating the scanning location. Both images show the ground surface with aquatic plants. DownScan™ (bottom right in Figure 11) was selected since it provided a relatively clearer view of the ground and vegetation, compared to Primary scan. Imagery display options, including contrast and brightness, horizontal scaling and color scheme, were selected within Reefmaster for maximum visual clarity.

Next, still hydroacoustic images were acquired at fixed time intervals using the MATLAB Toolbox 'Screen Record' by Nassim Khaled, which captures PC monitor contents in real-time. Playback of imagery at nine times the original speed expedited the capture process. The image capture rate was selected to achieve 20-30% spatial overlap between consecutive images. The toolbox code was modified to incorporate clock time instead of CPU time, creating images with consistent overlap by eliminating dependence on CPU load. Images were digitally masked and cropped to remove unnecessary information and facilitate the machine learning process (Fig. 12).

The top left portion of the image contains the GPS coordinates, while DownScan™ covers the remaining portion.

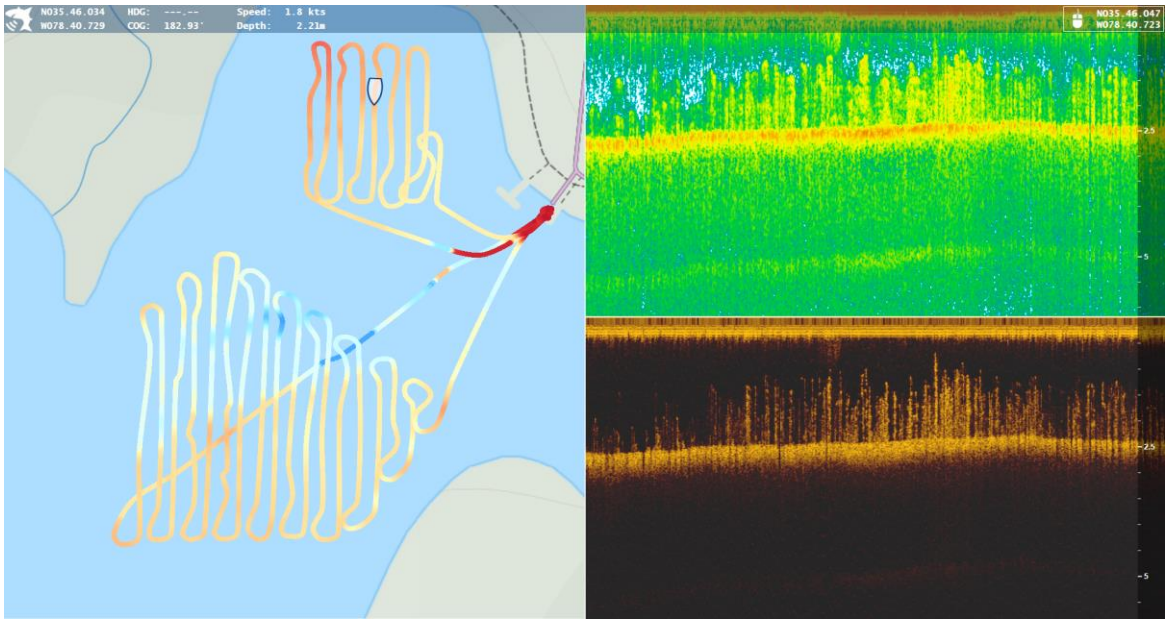

*Figure 11.* Screen shot from Reefmaster Sonar Viewer software illustrating hydro acoustic imagery acquired on Lake Raleigh: left -) map location corresponding with imagery (shown indicated by boat icon) and traversed path (with increasing depth, path color changes from red to blue); top right -) Primary scan sonar; and bottom right) - DownScan™ sonar.

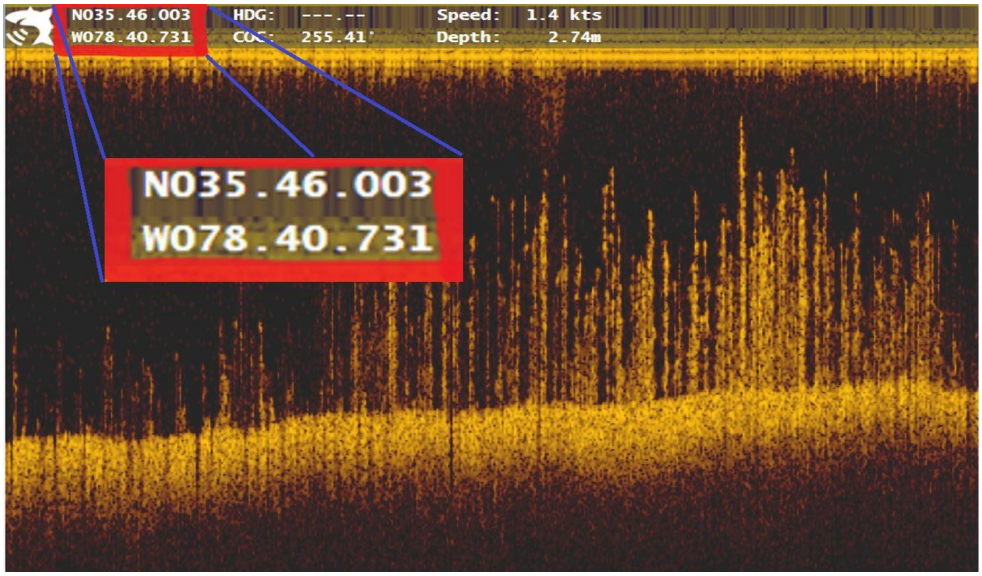


*Figure 12.* Geo-tagged DownScan™ Image with GPS coordinates in the top left corner.

### *2.2.2 Machine Learning Algorithm Development*

Initially, Python's OpenCV library was used for image preprocessing in an attempt to remove image artifacts such as the lake bed and water surface. However, due to the lack of image clarity (Fig. 13a and 13b), the processed images yielded a net loss of feature-defining information and failed to effectively remove these artifacts (Fig. 13c and 13d). Consequently, deep learning was employed to enable image classification without external image pre-processing. MATLAB was selected for deep learning implementation.

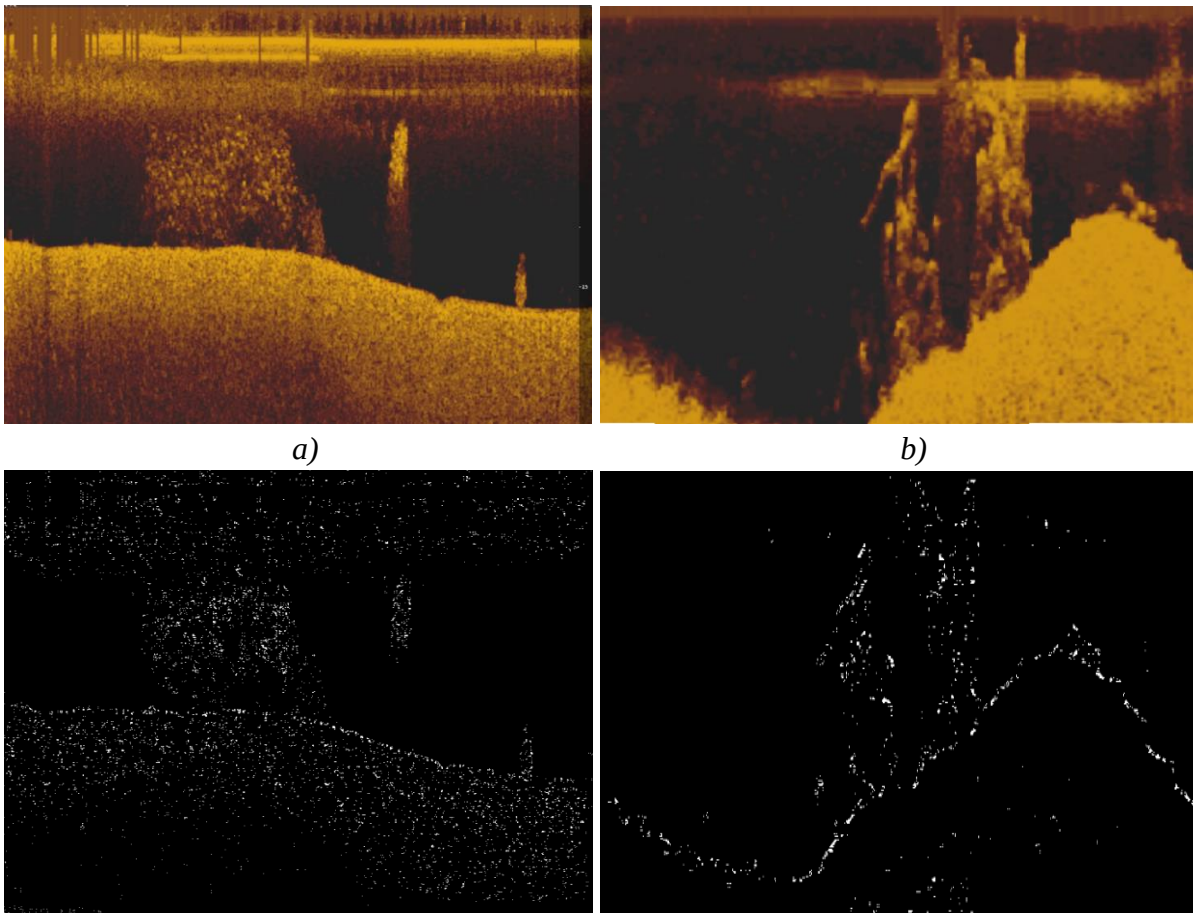

*a)* *b)*

*c)* *d)*

*Figure 13.* Image preprocessing attempts using the OpenCV library in Python: original hydroacoustic imagery of a) Hydrilla and b) Lyngbya; resulting imagery of c) Hydrilla and d) Lyngbya after image preprocessing.

### *2.2.3 Hardware and Software Configuration*

As noted earlier, DNNs, being computationally-intensive, require powerful processing units for training in a reasonable timeframe. DNNs have millions of learnable parameters which undergo hundreds/thousands of optimization cycles during training. This precludes the usage of standard CPUs, which have a limited number of cores (eight in typical desktop computers), for DNN training. However, modern GPUs, developed for gaming purposes, have thousands of cores which facilitate parallel computation via the Nvidia CUDA platform. For this research, a single Dell Precision T7500 workstation was configured with the following hardware: Intel Xeon CPU (2.13 GHz, 2 processors), 12GB RAM and Nvidia GTX 1070 Ti GPU with 8GB memory. The Nvidia CUDA Deep Neural Network (cuDNN) library and other supporting software was installed to enable MATLAB, Python and Google Colab to take advantage of the GPU.

### *2.2.4 DNN Training*

"Alexnet," an advanced CNN supported by MATLAB's Neural Network Toolbox, was used in the algorithm for plant species classification. Figure 14 shows the layer-wise structure of Alexnet. Due to a limited availability of preliminary data, initial algorithm training focused on only two training classes: the target species (Hydrilla: 466 images) and non-target species (Other: 1,751 images including some with no vegetation). Images of each class were randomly divided into training and validation sets (with 420 and 46 images, respectively). The DNN achieved 100% training accuracy, indicating sufficient network complexity. However, significant differences between training and validation accuracies indicated overfitting.

ANALYSIS RESULT

| | NAME | TYPE | ACTIVATIONS | TOTAL LEARNABLES |
|---|---|---|---|---|
| 1 | data | Image Input | 227×227×3 | 0 |
| 2 | conv1 | Convolution | 55×55×96 | 34944 |
| 3 | relu1 | ReLU | 55×55×96 | 0 |
| 4 | norm1 | Cross Channel Nor… | 55×55×96 | 0 |
| 5 | pool1 | Max Pooling | 27×27×96 | 0 |
| 6 | conv2 | Convolution | 27×27×256 | 307456 |
| 7 | relu2 | ReLU | 27×27×256 | 0 |
| 8 | norm2 | Cross Channel Nor… | 27×27×256 | 0 |
| 9 | pool2 | Max Pooling | 13×13×256 | 0 |
| 10 | conv3 | Convolution | 13×13×384 | 885120 |
| 11 | relu3 | ReLU | 13×13×384 | 0 |
| 12 | conv4 | Convolution | 13×13×384 | 663936 |
| 13 | relu4 | ReLU | 13×13×384 | 0 |
| 14 | conv5 | Convolution | 13×13×256 | 442624 |
| 15 | relu5 | ReLU | 13×13×256 | 0 |
| 16 | pool5 | Max Pooling | 6×6×256 | 0 |
| 17 | fc6 | Fully Connected | 1×1×4096 | 37752832 |
| 18 | relu6 | ReLU | 1×1×4096 | 0 |
| 19 | drop6 | Dropout | 1×1×4096 | 0 |
| 20 | fc7 | Fully Connected | 1×1×4096 | 16781312 |
| 21 | relu7 | ReLU | 1×1×4096 | 0 |
| 22 | drop7 | Dropout | 1×1×4096 | 0 |
| 23 | fc | Fully Connected | 1×1×2 | 8194 |
| 24 | prob | Softmax | 1×1×2 | 0 |
| 25 | classoutput | Classification Output | - | 0 |

*Figure 14.* Layer wise structure of Alexnet from MATLAB Neural Network Toolbox.

### *2.2.5 Reducing Overfitting*

The primary causes of overfitting include insufficient training data for generalization [Domingos, 2012] or excessive model complexity. Since the network structure already contained two dropout layers, data augmentation and model training with additional data were implemented to reduce overfitting [Srivastava, Hinton, Krizhevsky, Sutskever, & Salakhutdinov, 2014] [Krizhevsky, Sutskever, & Hinton, 2012]. Additional data was collected and Hydrilla images were generated with an increased overlap of approximately 50%, expanding the training and validation sets to 720 and 89 images, respectively. To implement data augmentation, artificial training data

was generated by modifying original images via horizontal reflection, translation and scaling. Furthermore, iterative parameter tuning was performed on optimization functions, learning rates, learning rate drop schedules, batch sizes and data augmentation parameters to increase classification accuracy.

### *2.2.6 Generalizing over multiple species*

Although image classification based on two classes (Hydrilla and Other) achieved satisfactory accuracy, classification across multiple plant species/classes was pursued to produce even better results with increased utility. To enable treatment of multiple species and enhance model generalization, hydroacoustic imagery of Cabomba and Coontail (ceratophyllum demersum), two common aquatic plant varieties, was collected and the DNN was trained on four classes. The data set was divided into training, validation, and test sets with 657, 80 and 80 images, respectively, of each class. Equal numbers of images in each class during training ensured prevention of sample bias; any significant difference was found to affect the classification probabilities. Cross verification on the test set following parameter tuning confirmed/ensured adequate model generalization.

### *2.2.7 Extracting GPS coordinates from images Post classification*

In conjunction with image classification, precise location of identified plant species is necessary for efficient treatment and recordkeeping. To create the required location database, the GPS coordinates superimposed on each hydroacoustic image (Fig. 13) were extracted using the Optical Character Recognition (OCR) functionality of MATLAB. Image preprocessing techniques, namely cropping, resizing, gray scaling and binarizing, enabled extraction of accurate GPS coordinates from the classified images (Fig. 22).

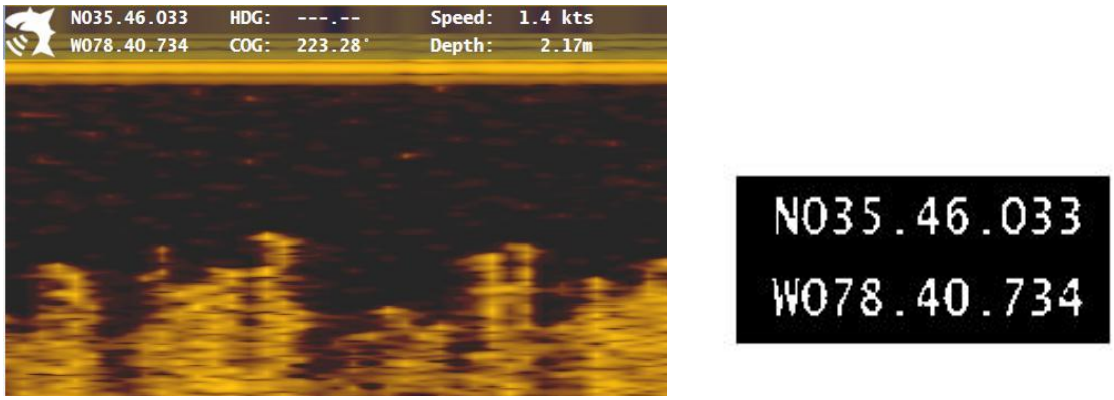


*a)* *b)*

*Figure 15.* GPS coordinate extraction with image preprocessing: a) raw/unprocessed hydroacoustic image and b) preprocessed image optimized for OCR. Generated output: N035 . 46.033↲W078 . 40 . 734↲↲.

# CHAPTER THREE:

# RESULTS

## 3.1 Autonomous Vehicle Performance

Autonomous water vehicles were deployed into multiple water bodies for a variety of weather conditions, spanning seasons from mid-summer to early winter. The majority of trials were conducted on Lake Raleigh, a 75-acre lake located on North Carolina State University's Centennial Campus, to evaluate the boats' manual and autonomous navigational capabilities and confirm the herbicide dispersal system functionality.

### *3.1.1 Autonomous Navigation*

With the marine propulsion system, prototypes achieved speeds up to 2.3 m/s and were able to navigate in the presence of moderate wind (4.5 m/s, 10 mph), light rain, and choppy surface water conditions. An iterative controller tuning process was completed to ensure high-performance tracking in autonomous navigation mode. Figure 15 shows autonomous tracking data for an earlier prototype with airboat-type propulsion (Fig. 15a) and a final generation prototype with marine propulsion (Fig. 15b). Intermittent, yet significant, tracking errors occurred with the airboat-propelled prototype due to wind gusts; these errors were not observed with marine propulsion. When the herbicide tank was filled to capacity, the maximum speed decreased, but minimal degradation in manual or autonomous navigation performance was observed.

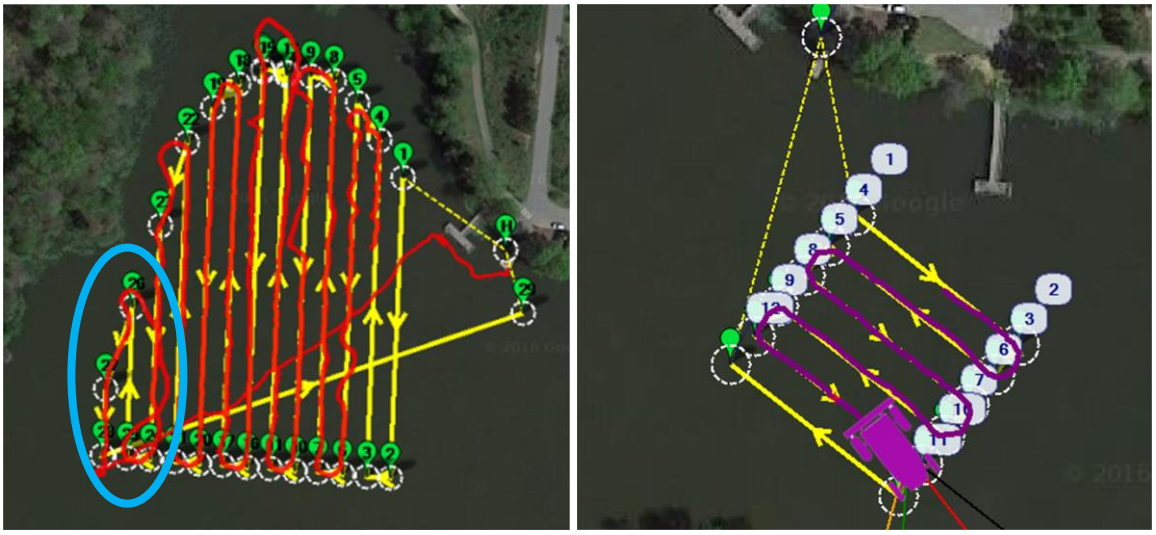

*a)* *b)*

*Figure 16.* Desired and actual trajectories for a) aircraft-propeller driven and b) marine-propeller driven prototypes after controller tuning. Poor tracking of the earlier prototype due to wind gusts are most noticeable in the circled region.

### *3.1.2 Battery Life*

Prototypes were powered by two 12-Volt lithium iron phosphate (LFP) batteries (Bioenno Power, Santa Ana, CA) wired in parallel, each rated at a 60 amp-hour capacity. While the batteries were not operated to depletion, data from multiple tests of over three hours suggests up to eight hours of operation time can be achieved on a single charge without falling below safe (80% discharge) levels.

### *3.1.3 Hydraulic Stability and Operational Depth*

Since the required submersion depth of the trolling motor exceeds the pontoon draft, the boat can be operated at any depth that can accommodate marine props. Nonetheless, with the prop motor positioned at minimal depth for shallow operation, angular travel of the vertical shaft (for steering purposes) must be software-limited to avoid collision of the blades with the pontoons during steering maneuvers. It must be noted that even with this angular limitation, adequate

navigation was achieved. Bow-to-stern inclination of the boat was minimal at all tank fill levels; the boat exhibited a slight, almost indiscernible, upward pitch (bow upward) at full tank capacity.

### *3.1.4 Herbicide Dispersal System*

Laboratory tests and computations, completed before lake tests, revealed that the dispersal system could provide moderate application rates of Aquathol-K (1.0-1.8 gal/A-ft) for typical pond depths, boat velocities, and transect widths. Figure 16 shows the range of chemical dispersal rates (Aquathol concentrate) achievable by varying the RC input, and the corresponding chemical concentrations (herbicide volume delivered per water body volume) for example herbicide applications. Optimal dispersal rate was further calculated for water body depth of 1.83 m (the USDA-recommended minimum depth in the southeastern United States), a boat speed of 1.0 m/s, and two transect options (6.1 and 9.1 m spacing).

Functionality of the dispersal system with chemical dilution modality was also demonstrated in Lake Raleigh; water was substituted for the herbicide to avoid unnecessary release of chemicals into the water body. Herbicide application was completed in a small (approximately 0.29 acres) private pond with watermeal infestation (Fig. 17). Due to the small surface area and volume of the pond, a premixed herbicide/water solution was dispersed directly from the tank and manual control, rather than autonomous navigation, was utilized.

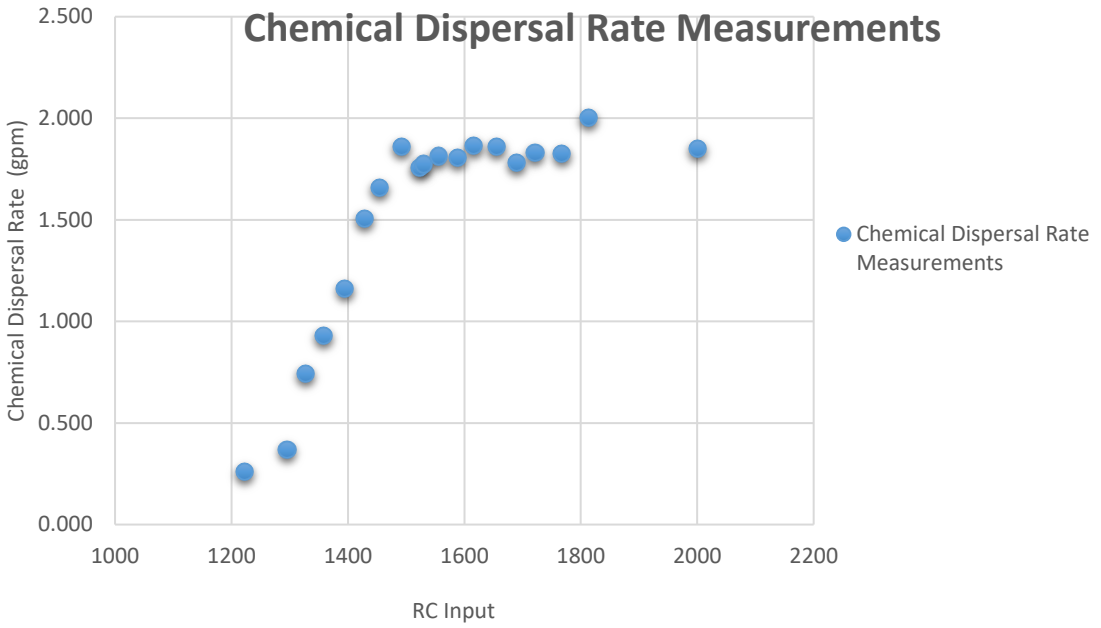


*Figure 17.* Characterization of chemical dispersal rates as a function of RC input.

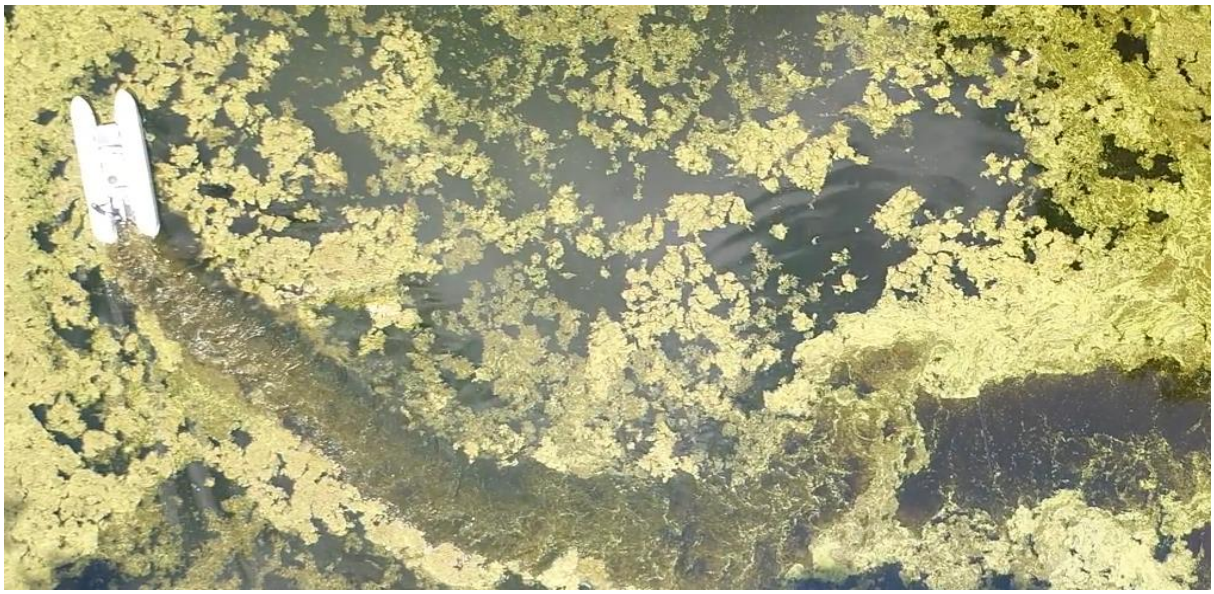

*Figure 18.* Treatment of watermeal infestation in a small pond using manual navigation and minimal prop submersion.

## 3.2 Machine Learning Algorithm

### *3.2.1 Vegetation Classification*

The deep learning algorithm, in conjunction with data augmentation, successfully extracted features and accurately classified underwater vegetation using hydroacoustic imagery. Figure 18 shows classification accuracy as a function of training iterations for both training and validation sets; it clearly illustrates how data augmentation reduced overfitting in the validation sets.

Initial parameter tuning readily improved the validation accuracy to approximately 97%; further parameter tuning produced only marginal gains. The optimizers ‘sgdm’, ‘rmsprop’ and ‘adam’ gave similar performance, with ‘sgdm’ and ‘adam’ producing marginally better accuracy. Increased smoothness of the training curve and improved accuracy were observed for all optimizers by reducing the learning rate. A learning rate drop schedule further improved the accuracy as compared to a constant learning rate. The “MiniBatch Size” parameter contributed heavily to runtimes and smoothness of the training curve. Greater batch sizes smoothed the curve and reduced runtimes but increased the memory requirements. Limiting batch sizes to 256 or less helped avoid the “sharp minimizers” that tend to impede generalization [Keskar, Mudigere, Nocedal, Smelyanskiy, & Tang, 2017].

Following parameter tuning, the DNN achieved a classification accuracy of 99.06% for both the validation and test data sets, clearly indicating excellent generalization. Analysis of the confusion matrices for different tuning parameters revealed more misclassifications within the Hydrilla and Other classes (and between the two) than within the Cabomba and Coontail classes. Figure 19 shows the confusion matrices for the optimal parameter set.

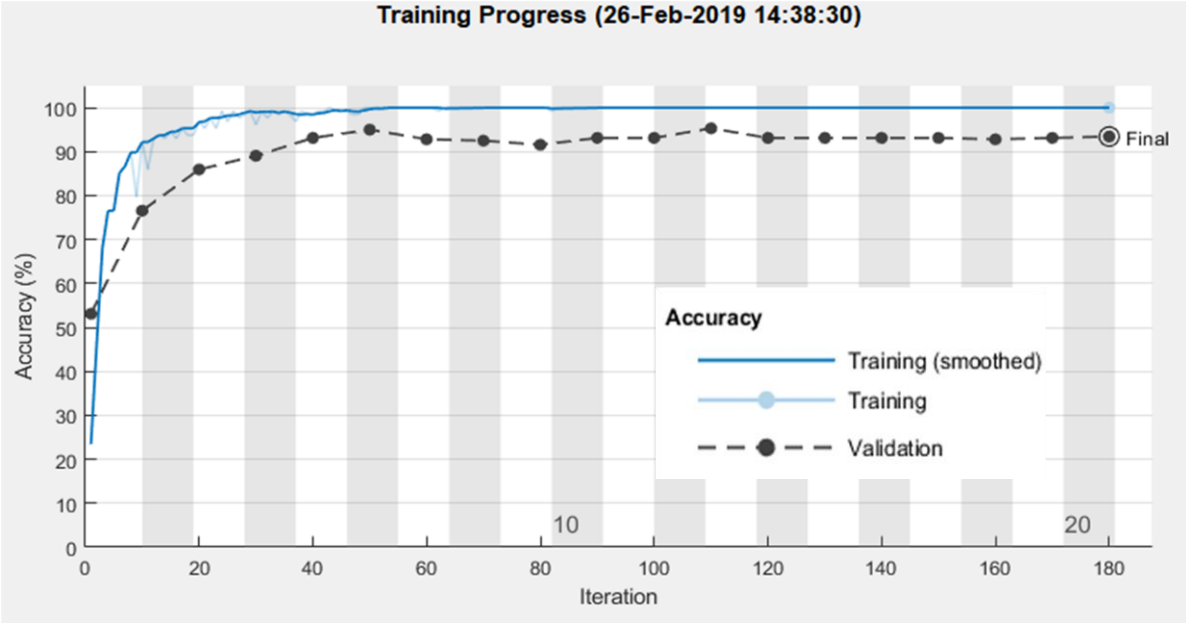


*a)*

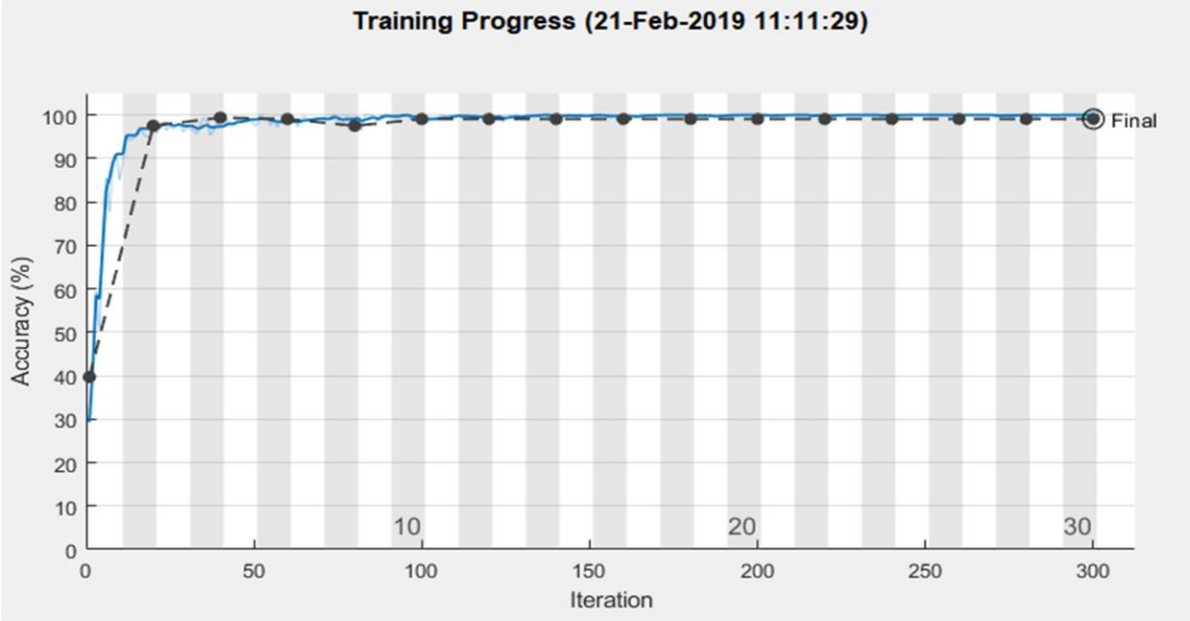


*b)*

*Figure 19.* Training progress a) before and b) following data augmentation. Overfitting in a) is evident through high variation between training and validation accuracy.

Subsequent analysis revealed that misclassified Hydrilla images tended to be associated with limited plant growth (Fig. 20a). The majority of images containing Cabomba and Coontail were associated with more mature plant growth, which perhaps led to higher classification

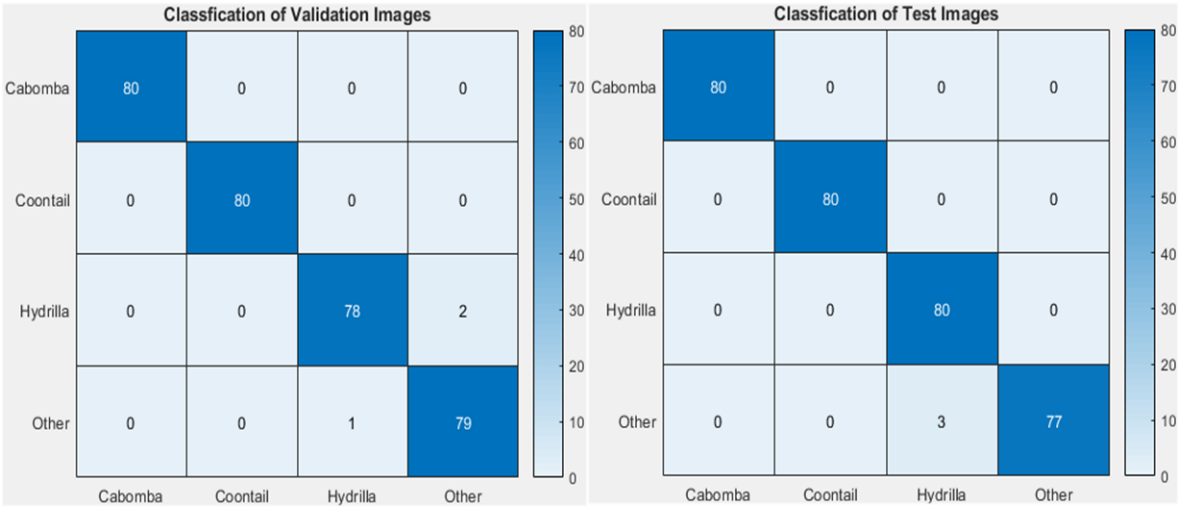


*a)* *b)*

*Figure 20.* Confusion matrices of classified vegetation species for validation (a) and test images (b).

accuracies. This suggests that timing of data capture within the growing season might play an important role in classification accuracy. Data for Hydrilla was collected from June to November while Cabomba and Coontail were scanned during December, a time of year associated with more mature growth. Other instances of misclassification included images containing floating vegetation or schools of fish (Fig. 20b), and vegetation being only partially contained within the image (Fig. 20c).

During DNN training, weights of all layers undergo continuous optimization. Successful feature learning creates smooth filters with uniform weight gradients. Figure 21 visualizes the 96 filters (each with 11 × 11 × 3 weights) of the first convolutional layer for two separate cases. Parameter tuning generated smoother, blended (less discretized) gradient patterns, which are characteristics of effective training (Fig. 21b), while filters in Figure 21a indicate lack of sufficient training.

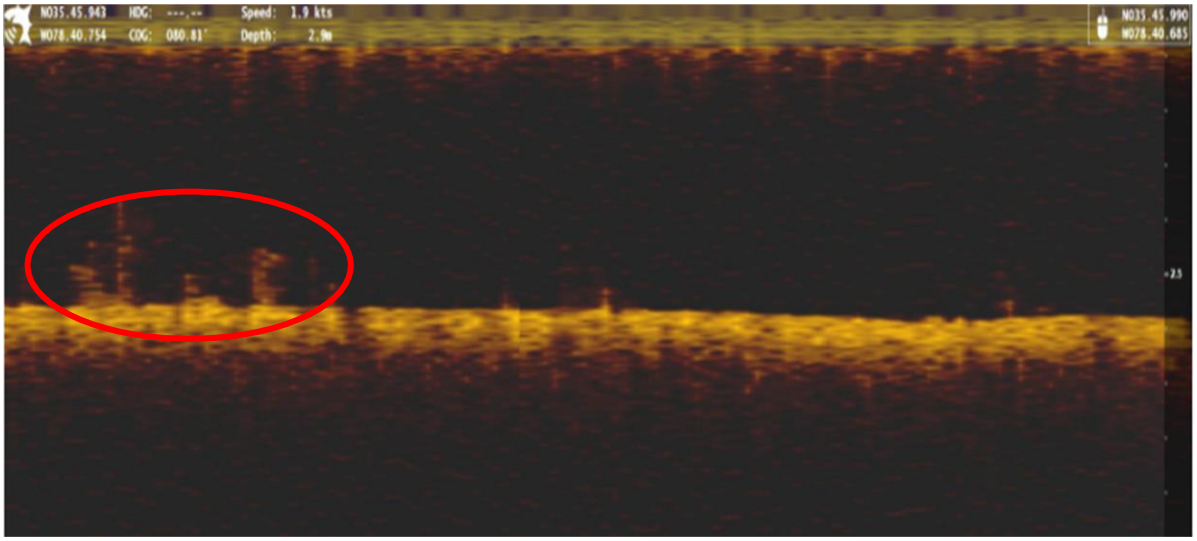


*a)*

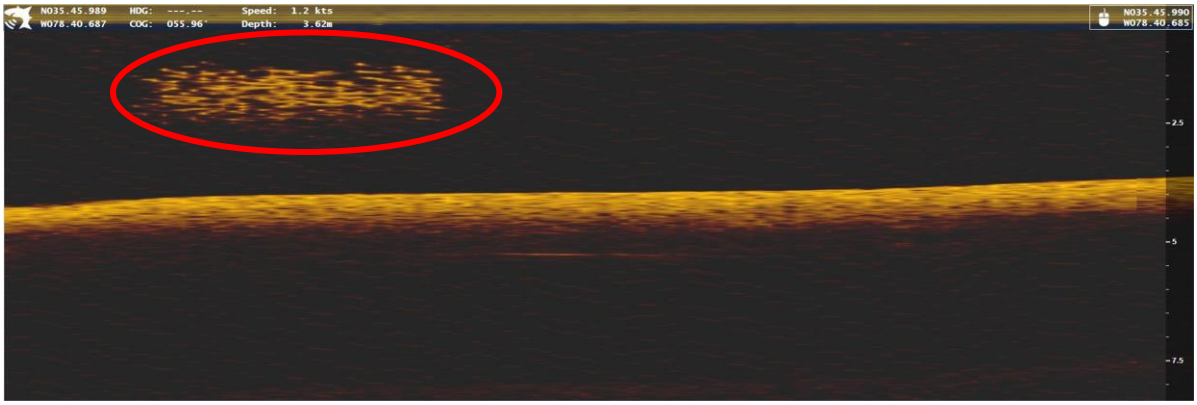


*b)*

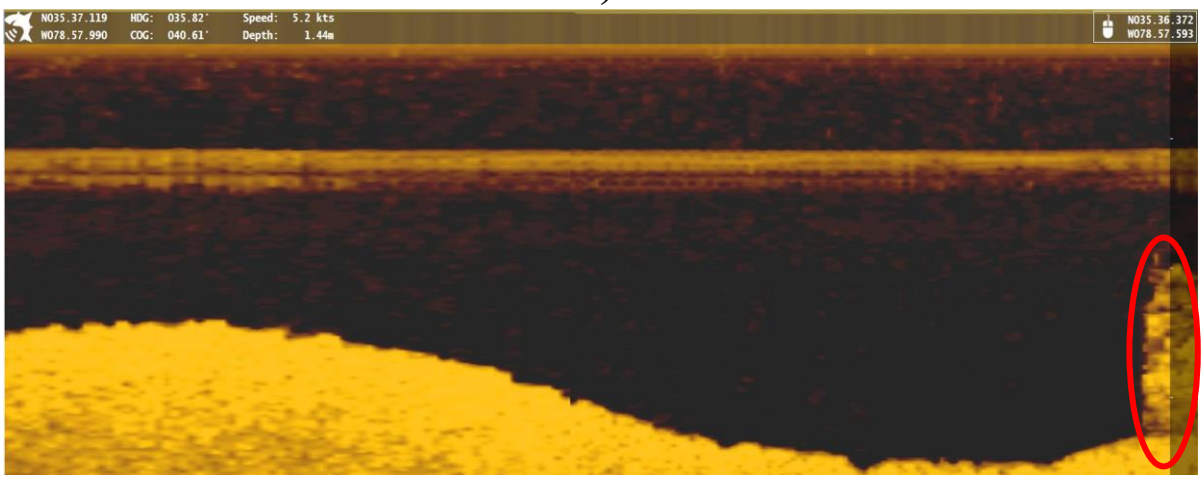


*c)*

*Figure 21.* Misclassified images due to a) limited vegetation growth, b) floating vegetation or schools of fish, and c) partial/narrow vegetation contained within the image.

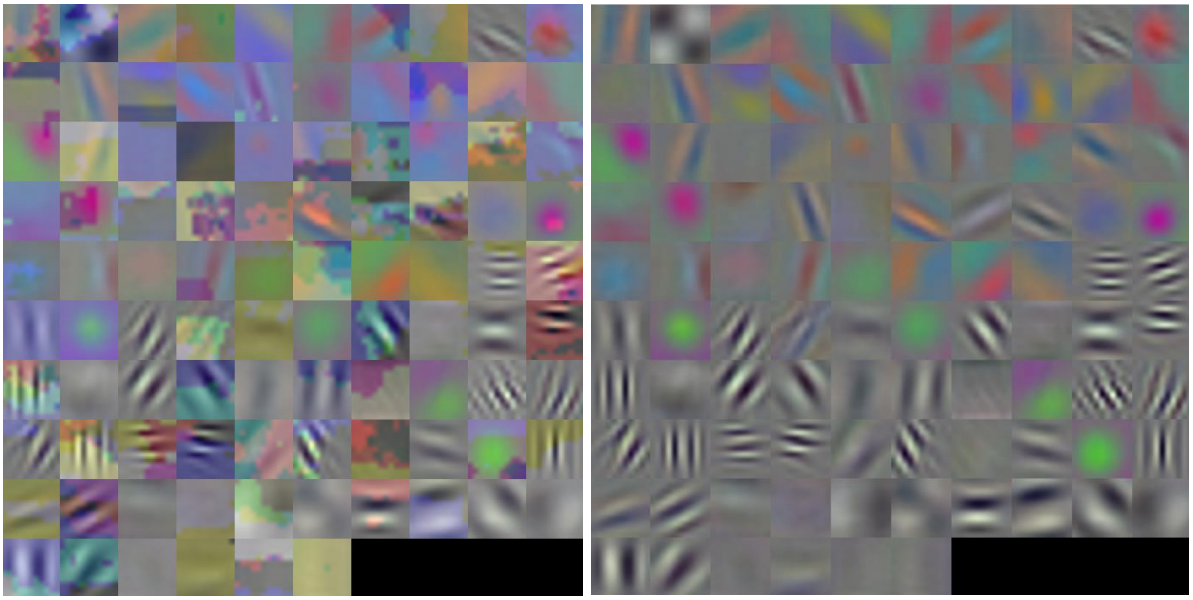

*a)* *b)*

*Figure 22.* DNN weight visualization for first convolutional layer a) before parameter optimization and b) after training with parameter optimization.

# CHAPTER FOUR:

# DISCUSSION

This research was successful in developing the necessary hardware and software for automated identification and treatment of submerged aquatic weeds. A small fleet (two watercraft) with the required systems and capabilities (self-navigation, hydroacoutic data collection and herbicide dispersal) were developed over three prototype generations. Hydrilla, being a very invasive weed species with severe impacts, was chosen as the targeted aquatic weed. The deep learning model was later extended to multiple species, namely Hydrilla, Cabomba and Coontail (four classes in total, including 'Other'). High classification accuracy of 99.06% on both the validation and test sets indicate excellent generalization. Training on four classes with a higher volume of data improved the algorithm accuracy as compared to training on two classes. Geotagged information from classified images was reliably extracted for treatment of the target areas with herbicides.

While the integration of autonomous scanning, identification and treatment of invasive plant species was to some extent limited by software and hardware capabilities, the current practice of manually scanning and treating entire water bodies can be eliminated using this approach. The technologies detailed here clearly have the potential to reduce the cost and increase the effectiveness of aquatic plant management.

## 4.1 Future Work

Because plant maturity was found to have an impact on classification accuracy, it may be advisable to collect data of each plant variety throughout the growing season and at multiple locations to help further generalize the model. Future research will likely focus on improved hardware and software integration, which will enable synchronous execution of all system tasks: hydroacoustic data collection, weed classification and distribution mapping, and targeted herbicide treatment. The integrated process would involve automated weed classification during hydroacoustic scanning, which could be accomplished through one of several methods. The first option involves performing all classification and location extraction tasks on a central computer, located with the operator. In this option, the hydroacoustic data could be transferred to the central computer using existing hydroacoustic wireless technology, e.g., the "Navico gofree wifi1" wireless module (Navico Marine Electronics, Egersund, Norway), or a Wi-Fi enabled SD card. To overcome limited transmission range, transects could be configured to periodically direct boats close to the operator for wireless data transmission. Post weed classification and target location identification by the computer, an operator could generate transects covering these locations and transmit them to the vehicles for herbicide application. Multiple boats could be employed simultaneously for weed detection and treatment with a single operator (based on the shore or in another watercraft, e.g. canoe or motorized craft).

The second option involves the use of onboard computer processing systems, e.g., Raspberry Pi units or tablets, for real-time image classification. Live data could be transferred from the terminals of the fish finder to the processor using Wireshark software [A. Debrowski, 2011]. The herbicide application system could be triggered immediately upon detection of targeted weed species. Applying this methodology, scanning and treatment could be completed in a single

completion of the transects. In spite of its benefits, this method would require extensive research to successfully configure real-time communication between software (Wireshark, Reefmaster, MATLAB, Mission Planner) and hardware components (hydroacoustic scanner, autopilot module, etc.).

## REFERENCES


1. Hydrilla verticillata (L.F.) Royle (Hydrocharitaceae), "The Perfect Aquatic Weed", Kenneth A. Langeland, Castanea, Vol. 61, No. 3 (Sep., 1996), pp. 293-304, Southern Appalachian Botanical Society

2. L. A. Helfrich, R.J. Neves, G. Libey, T. Newcomb (2009). “Control Methods For Aquatic Plants in Ponds and Lakes”, Publication 420-251, Virginia Cooperative extension

3. Jones, B. 2013, ‘Plane: L1 Control for Straight and Curved Path Following’, GitHub, blog post, viewed 2 January 2015, <https://github.com/ArduPilot/ardupilot/pull/101>.

4. Beverly, G 2017, ‘Development and Experimentation of an Herbicide Dispersal System for an Autonomous Aquatic Weed Management System’, MS thesis, North Carolina State University, <https://repository.lib.ncsu.edu/handle/1840.20/34395>.

5. C. Lembi, (2009), “Identifying and Managing Aquatic Vegetation”, Purdue Extension, APM-3-W

6. L. Pereira, R. Nakamura, G. de Souza, D. Martins, J. Papa (2012) “Aquatic weed automatic classification using machine learning techniques”, Elsevier, Computers and Electronics in Agriculture 87 (2012) 56-63

7. S. J. Kho, S. Manickam, S. Malek, M. Mosleh & S. K. Dhillon (2017) “Automated plant identification using artificial neural network and support vector machine”, Frontiers in Life Science, 10:1, 98-107

8. S. Park, J. Deyst, and J. P. How, "A New Nonlinear Guidance Logic for Trajectory Tracking," Proceedings of the AIAA Guidance, Navigation and Control Conference, Aug 2004. AIAA-2004-4900.

9. Y. Sun, Y. Liu, G. Wang, H. Zhang (2017), “Deep Learning for Plant Identification in Natural Environment”, Hindawi, Computational Intelligence and Neuroscience, Vol: 2017, Article: 7361042

10. J. Baron, D. Hill, H. Elmiligi (2018), “Combining image processing and machine learning to identify invasive plants in high- resolution images”, International Journal of Remote Sensing, DOI: 10.1080/01431161.2017.1420940

11. W. Liua, Z. Wanga, X. Liua, N. Zengb, Y. Liuc, F. Alsaadid (2017), “A survey of deep neural network architectures and their applications”, ELSEVIER, Neurocomputing 234 (2017) 11–26

12. C. Hung, Z. Xu, S. Sukkarieh (2014), “Feature Learning Based Approach for Weed Classification Using High Resolution Aerial Images from a Digital Camera Mounted on a UAV”, Remote Sensing. 2014, 6, 12037-12054; doi:10.3390/rs61212037

13. P. Domingos (2012), “A Few Useful Things to Know About Machine Learning”, Communications of the ACM, October 2012, Vol. 55, No. 10

14. N. Srivastava, G. Hinton, A. Krizhevsky, I. Sutskever, R. Salakhutdinov (2014), “Dropout: A Simple Way to Prevent Neural Networks from Overfitting”, Journal of Machine Learning Research 15 (2014) 1929-1958

15. Krizhevsky, I. Sutskever, G. Hinton (2012), “Advances In Neural Information Processing Systems”, Advances In Neural Information Processing Systems, arXiv:1102.0183

16. N. Keskar, D. Mudigere, J. Nocedal, M Smelyanskiy, P. Tang (2017), “On Large-Batch Training For Deep Learning : Generalization Gap And Sharp Minima”, ICLR, arXiv:1609.04836v2 [cs.LG] 9 Feb 2017

17. A. Debrowski, S. Busch, R. Stelzer (2011), “A digital Interface for Imagery and Control of a Navico/Lowrance Broadband Radar”, Springer, DOI: 10.1007/978-3-642-22836-0_12